The Oxygen Release Instrument: Space Mission Reactive Oxygen Species Measurements for Habitability Characterization, Biosignature Preservation Potential Assessment, and Evaluation of Human Health Hazards

Christos D. Georgiou [1,*], Christopher P. McKay [2] , Richard C. Quinn [3], Electra Kalaitzopoulou [1,†], Polyxeni Papadea [1,†] and Marianna Skipitari [1,†]

[1] Department of Biology, University of Patras 26504, Greece
[2] NASA Ames Research Center, Moffett Field, CA 94035, USA
[3] SETI Institute, Carl Sagan Center, Mountain View, CA 94043, USA
[*] Correspondence: c.georgiou@upatras.gr; Tel.: +30-2610-997-227; Fax: +30-2610-969-278
[†] These authors contributed equally to this work.

Abstract: We describe the design of an instrument, the OxR (for Oxygen Release), for the enzymatically specific and non-enzymatic detection and quantification of the reactive oxidant species (ROS), superoxide radicals ($O_2^{\bullet-}$), and peroxides (O_2^{2-}, e.g., H_2O_2) on the surface of Mars and Moon. The OxR instrument is designed to characterize planetary habitability, evaluate human health hazards, and identify sites with high biosignature preservation potential. The instrument can also be used for missions to the icy satellites of Saturn's Titan and Enceladus, and Jupiter's Europa. The principle of the OxR instrument is based on the conversion of (i) $O_2^{\bullet-}$ to O_2 via its enzymatic dismutation (which also releases H_2O_2), and of (ii) H_2O_2 (free or released by the hydrolysis of peroxides and by the dismutation of $O_2^{\bullet-}$) to O_2 via enzymatic decomposition. At stages i and ii, released O_2 is quantitatively detected by an O_2 sensor and stoichiometrically converted to moles of $O_2^{\bullet-}$ and H_2O_2. A non-enzymatic alternative approach is also designed. These methods serve as the design basis for the construction of a new small-footprint instrument for specific oxidant detection. The minimum detection limit of the OxR instrument for $O_2^{\bullet-}$ and O_2^{2-} in Mars, Lunar, and Titan regolith, and in Europa and Enceladus ice is projected to be 10 ppb. The methodology of the OxR instrument can be rapidly advanced to flight readiness by leveraging the Phoenix Wet Chemical Laboratory, or microfluidic sample processing technologies.

Keywords: planetary oxygen-based reactive oxidants; instrument; habitability; biosignatures

1. Introduction

On Earth, the production of reactive oxygen species (ROS) in soils is typically associated with the relatively high abundance of $O_2(g)$ in the atmosphere [1]. In other solar system environments, or space environments beyond our solar system, where $O_2(g)$ exists only in trace amounts (e.g., Mars [2], the Earth's Moon [3,4], Europa [5], Saturn's rings [6], interstellar clouds [7]) the production and accumulation of ROS is not precluded.

Even in planetary environments lacking $O_2(g)$, ROS can be produced by many well-known natural processes, for example, environments containing H_2O, CO, and/or CO_2 [8]. On the Moon (and presumably on Mars), ROS can be generated by the interaction of H_2O ice with cosmic rays [9]. Experiments indicate that Lunar (and presumably Martian) dust can generate hydroxyl free radicals ($^{\bullet}OH$) via the Fenton reaction as demonstrated with Lunar simulants [10] and Fe-rich silicate

minerals [11]. Freshly fractured Lunar regolith can produce large amounts of H_2O_2 and other ROS [12], which are considered to play a role in Lunar dust toxicity [13]. Although, none of the curated Apollo mission Lunar samples exist in a state that fully preserves the reactive chemical surfaces aspects (i.e., ROS) that would be expected to be present on the lunar surface, freshly ground Lunar soil has been shown to produce $^•OH$ upon contact with H_2O [14]. On Mars, reactive O_2^+ and O_2^- can form through the release of reactive oxygen via scattering of CO_2 ions from solid surfaces; where oxygen produced is preferentially ionized by charge transfer from the surface over the predominant atomic oxygen product [8]. ROS may also be produced by Martian regolith via silicate abrasion during dust storms [15] (e.g., by mechano-radical production [16]). Silica fracturing is known to generate surface free radicals (homolytic and heterolytic fracturing form $Si^•/SiO^•$, and Si^+/SiO^-, respectively), which upon reaction with H_2O or H_2O_2 generate $^•OH$ [17]. Such dust/silica-induced radicals may pose a serious human health hazard (verified by toxicity studies on mammalian cells [18]), during future manned missions to Mars and Moon.

Beyond Mars and the Moon, complex interactions between Saturn and its satellites Titan and Enceladus can cause the generation and movement of oxygen from the latter to the former [19,20]. Ice water from Enceladus south polar plumes can be radiolytically oxidized to H_2O_2 and O_2, by energetic particles from Saturn's radiation belts (mostly electrons). Such ROS emanating from this radiolytic gas-driven cryovolcanism can be continuously accumulated deep in icy regolith [19]. Concurrently, H_2O molecules escaping from Enceladus' plumes should be split by magnetospheric plasma (protons, H^+_2, water group ions) into neutral and charged particles (O^+), which can enter Titan's atmosphere and be captured by fullerenes (a hollow carbon atom shell, e.g., of C_{60}). Exogenic keV O^+ could become free oxygen within those fullerene aerosols, and eventually, fall free onto Titan's surface. Such a process could be driven by cosmic ray interactions with aerosols at all heights, and can eventually, drive pre-biotic chemistry [20]. It has been suggested that ice-covered worlds require an external source of oxidants to maintain biological viability [21]. Hand et al. 2007, have proposed that oxidants produced by UV and ionizing radiation on the surface of icy worlds, such as Europa, can be carried down to the water column to react with reduced species to provide a source of redox energy [22].

In light of all these considerations, measurement of planetary ROS is of great interest for astrobiology, including the exploration of Titan, Enceladus, and Europa, and important for human missions to the Moon and Mars. However, instruments for the in situ specific detection of the key ROS $O_2^{•-}$ and O_2^{2-} (e.g., H_2O_2) in these extreme environments have not yet been developed.

The justification for this type of instrument is supported by the results of the Viking Mars mission. In 1976, the Viking Lander performed biological experiments designed to detect extant life in Martian regolith. The reactivity of the Martian regolith was first indicated by the release of O_2 in the Gas Exchange Experiment (GEX), and the decomposition of organics, contained a culture media, in the Labeled Release (LR) experiment [23–25]. In the GEX, up to ~770 nmoles $O_2(g)$ was produced from regolith samples (1 cm^{-3}) upon humidification or wetting. The persistence of $O_2(g)$ release from samples that were heated to 145 °C for 3 h and then cooled prior to wetting or humidification, ruled out a biological explanation of the GEX results [23,26]. In the Viking LR, up to ~30 nmoles ^{14}C labeled gas, presumed to be CO_2, was released after regolith samples (0.5 cm^{-3}) were wetted with an aqueous solution containing ^{14}C-labeled organics [27,28]. The release of ^{14}C-labeled gas in the LR was eliminated by heating the sample to 160 °C for 3 h and then cooling prior to the addition of the labeled aqueous organics. These results lead to the conclusion that the Martian surface material contains more than one type of reactive oxidants [23]. Metal salts of $O_2^{•-}$ were among the earliest proposed explanations for the thermally stable agent responsible for $O_2(g)$ release in the GEX. In the case of the LR, peroxide was among the earliest explanations proposed for the thermally liable agent responsible for $^{14}CO_2$ release. In addition to the possible presence of metal salts of $O_2^{•-}$, it has been proposed that $O_2^{•-}$ is generated on Martian dust and regolith surfaces by a UV-induced mechanism [29]. Such a mechanism for $O_2^{•-}$ photo-generation has also been shown with Mars analog Mojave and Atacama regolith [1].

More recently, high levels of regolith perchlorate (ClO_4^-) were directly detected at the Phoenix landing site [30]. Following up on this result, the presence of ClO_4^- at the Viking landing sites was inferred [31], and its presence at the Martian equator verified by the Sample Analysis at Mars (SAM) instrument on Mars Science Laboratory (MSL)-based on thermal analyses [32]. While the stability of ClO_4^- under the conditions of the GEX and LR preclude it as a direct explanation for these experiments, it has been suggested that ClO_4^- radiolysis products reproduce the major aspects of both experiments [25]. The form of the trapped O_2, in particular, derived from ClO_4^- radiolysis, was not identified, and it has been suggested that some fraction may exist as superoxide radical or peroxide [25,33]. This suggestion was confirmed by the finding that both of these oxidants are generated—together with $^\bullet OH$—by γ-ray exposure of ClO_4^- (mixed in Mars salt analogs) upon water wetting [34]. Preceding this finding, other possible oxidants present on the surface of Mars have been reviewed in detail [35]. In the context of instrument development for in situ analysis, it is useful to note that the expected concentration of oxidants, as inferred from the Viking Biology Experiments, is at the parts per million level (Table 1 in [36]).

Given the poorly understood nature and distributions of oxidants in Martian and Lunar regolith, there is a need for the development of flight instruments for their specific identification and quantification. The only flight instrument previously built for the quantitative, although non-specific, in situ determination of oxidants was the Mars Oxidant Experiment (MOX) instrument [36] as the United States contribution to the failed Soviet Union's Mars '96 mission. That instrument would have exposed materials-sensors to the Martian regolith and monitored their reaction with oxidants over time. Materials included various metallic (e.g., Al, Ag, Pb, Au) and organic layers (e.g., L- and D-cysteine).

New developments have made possible the detection of reactive oxidants, such as peroxides (O_2^{2-}), $O_2^{\bullet-}$, and $^\bullet OH$ [1,34]. In planetary and terrestrial regolith, $O_2^{\bullet-}$ may exist as adsorbed ($O_2^{\bullet-}{}_{ads}$) [1] or present in metal salts ($Me^+ O_2^{\bullet-}$), such as KO_2 and NaO_2 [37], and in ionic complexes with metals ($Me^{n+} - O_2^{\bullet-}$) of certain minerals and oxides [38,39]. Metal peroxides can exist as salts of metals with O_2^{2-} bonding either as $Me^{2+}O_2^{2-}$ (e.g., CaO_2, MgO_2) or as $Me^+{}_2O_2^{2-}$ (e.g., Na_2O_2, K_2O_2). Metal peroxides can also exist as hydroperoxides (MeO_2H; e.g., of Ti^{4+}, Zr^{4+}, and Ce^{4+}) [40]. The presence of Mg^{2+}, Ca^{2+}, K^+, and Na^+ ions on Martian regolith (measured with the Phoenix Mars Lander Wet Chemistry Lab [30,41,42]) and on Lunar regolith [43], may provide the needed counter ions for stabilization of metal salts of $O_2^{\bullet-}$, peroxides, and hydroperoxides in the regolith. Metal salts of $O_2^{\bullet-}$ and hydro/peroxides (i.e., O_2^{2-}) can undergo aqueous decomposition at neutral pH, releasing O_2 and H_2O_2 (Table 1).

Table 1. Aqueous decomposition of metal salts of $O_2^{\bullet-}$ and O_2^{2-}

Metal (Me) Salts of $O_2^{\bullet-}$ Release O_2 (↑) and H_2O_2 by the Following Reactions [37,44]		
Adsorbed $O_2^{\bullet-}$	$2\,O_2^{\bullet-}{}_{ads} + 2\,H_2O \rightarrow 2\,OH^- + H_2O_2 + O_2\uparrow$	(1)
Metal salts of $O_2^{\bullet-}$	$2\,Me^+\,O_2^{\bullet-} + 2\,H_2O \rightarrow 2\,Me^+OH^- + H_2O_2 + O_2\uparrow$	(2)
Metal-$O_2^{\bullet-}$ complexes	$2\,Me^{n+} - O_2^{\bullet-} + 2\,H_2O \rightarrow 2\,Me^{n+} + 2\,OH^- + H_2O_2 + O_2\uparrow$	(3)
Metal Peroxides/Hydroperoxides Release H_2O_2 by the Following Reactions [37]		
Me-salts of O_2^{2-}	$Me^+{}_2O_2^{2-} + 2\,H_2O \rightarrow 2\,Me^+OH^- + H_2O_2$	(4)
	$Me^{2+}O_2^{2-} + 2\,H_2O \rightarrow Me^{2+}(OH^-)_2 + H_2O_2$	(5)
Me-hydroperoxides (MeO_2H)	$MeOOH + H_2O \rightarrow MeOH + H_2O_2$	(6)

2. Principle of Operation of the OxR (for Oxygen Release) Instrument

The OxR instrument for the detection and quantification of $O_2^{\bullet-}$ and O_2^{2-} addresses priorities for human exploration of Mars and the Moon as highlighted in the NASA plan to "Explore Moon to Mars" which will use the Moon as "a testbed for Mars [. . .] and beyond." [45].

Our approach is to quantitatively convert peroxides and superoxide radicals into $O_2(g)$, which can then be detected easily, precisely, and with very high sensitivity. The principle of the OxR instrument is based on the enzymatic conversion of the dismutation and hydrolysis products of superoxide radicals ($O_2^{\bullet-}$ adsorbed on

mineral surfaces, $O_2^{\bullet-}{}_{ads}$, or released by the dissociation of metal salts of $O_2^{\bullet-}$) and peroxide (O_2^{2-} as H_2O_2 or released by the hydrolysis of metal peroxides) to O_2, followed by quantitative detection using an O_2 electrode.

The OxR instrument design includes a sealable, temperature- and pressure-controlled sample chamber. The chamber is equipped with an O_2-sensor, and inlets for the sequential dispensing of three reagents, after each of which the concentration of released O_2 is measured. The two enzymatic reagents (Cu/Zn-superoxide dismutase, SOD, and catalase, CAT) used are stored in a solid form separated from their aqueous solvents (to withstand cosmic radiation exposure). The third reagent, acetonitrile (ACN), is separately stored at any temperature above its melting point ($-46°C$). The enzymic reagents are mixed with their solvents right before use either by storing them in separate reagent crucibles (analogous to those used in the Wet Chemistry Laboratory of the 2007 Phoenix Mars Scout Lander mission), or in (commercially available) dual-chamber pre-fillable syringes (one chamber for storing the enzyme reagent in solid form, and the other for its solvent, to be mixed upon piston movement), and their sequential dispensing in the chamber. The OxR instrument can detect released O_2 by electrochemical or solid state optical O_2-sensing electrodes. Both electrode types are commercially available. Optical O_2-sensing electrodes are based on the luminescence quenching by O_2, and are sensitive enough to measure O_2 at ~1 nmole O_2 per cubic cm (cm^{-3}) of regolith or water, i.e., much lower than that detected by the GEX (775 nmoles cm^{-3} regolith). This translates to a minimum instrument detection limit for metal salts of $O_2^{\bullet-}$ and O_2^{2-} of 0.01 ppm (= 10 ppb) for Martian and Lunar regolith or O_2^{2-} in Europa and Enceladus water. This sensitivity corresponds to ~10 μg $O_2^{\bullet-}/O_2^{2-}$ kg^{-1} Mars or Lunar surface regolith (based on a density of 1.4–1.6 g cm^{-3} for Mars [46,47], and for the Moon [48]).

3. Enzyme-Based ROS Specificity of the OxR Instrument

We have developed an enzymatic methodology (OxR assay) for the detection of total $O_2^{\bullet-}$ (the sum of $O_2^{\bullet-}{}_{ads}$, $Me^+ O_2^{\bullet-}$, and $Me^{n+} - O_2^{\bullet-}$) and total O_2^{2-} (the sum of $Me^{2+}O_2^{2-}$, $Me^+{}_2O_2^{2-}$, and MeO_2H), for terrestrial field and planetary applications [49]. The use of enzymes for the OxR assay provides specificity and quantification of regolith $O_2^{\bullet-}$ (reactions 1–3) and O_2^{2-} (reactions 4–6) through the measurement of the O_2 that is enzymatically released during dismutation/hydrolysis. Specifically, this is achieved using the following enzymatic reactions [44]: (i) the SOD-catalyzed dismutation of 1 mole $O_2^{\bullet-}$ to ½ mole O_2 and ½ mole H_2O_2, and (ii) the CAT-decomposition of 1 mole H_2O_2 (from dismutated $O_2^{\bullet-}$ and hydrolyzed metal peroxides/hydroperoxides) to ½ mole O_2.

The enzymatic reaction steps of the OxR assay have been established by the following experimental testing [49]: (i) The effective scavenging of $O_2^{\bullet-}$ via dismutation to O_2 and H_2O_2 by SOD; (ii) the decomposition of H_2O_2 (from the hydrolysis of peroxides and the dismutation of $O_2^{\bullet-}$) to O_2 (by CAT) in the presence of ClO_4^- and carbonate (CO^{2-}; both Martian regolith constituents), and in potassium phosphate plus diethylene–triamine–pentaacetic acid (DTPA) buffer (pH 7.2). Phosphate is an H_2O_2-stabilizer [50], and DTPA acts as chelator of any soluble transition metal ions, which can destroy H_2O_2 via the Fenton reaction [51] and $O_2^{\bullet-}$ via oxidation to O_2); (iii) the functional stability of the OxR assay enzymes SOD and CAT to cosmic rays upon exposure to γ-radiation; (iv) the simulation of the OxR assay by indirect testing on commercial analogues of metal salts of $O_2^{\bullet-}$ and O_2^{2-}, and directly on $O_2^{\bullet-}$ and H_2O_2. The enzymatic (and accompanying non-enzymatic) reactions involved in the OxR assay are presented in Table 2.

Table 2. Reactions of the OxR (Oxygen Release) assay.

I. Metal $O_2^{\bullet-}$ ($O_2^{\bullet-}{}_{ads}$, $Me^+ O_2^{\bullet-}$, $Me^{n+}-O_2^{\bullet-}$); additional details for their hydrolysis/dismutation are presented in reactions 1–3, and in Figure 1 *step a*.	Step 1. Metal $O_2^{\bullet-}$ (e.g., $Me^+ O_2^{\bullet-}$) dissociation reaction: $Me^+ O_2^{\bullet-}$ (in H_2O) → $O_2^{\bullet-} + Me^+$ *Note*: Stock solution of stable $O_2^{\bullet-}$ is obtained by dissociation of $Me^+ O_2^{\bullet-}$ (e.g., KO_2) in anhydrous acetonitrile (ACN). Step 2. Release of O_2 (and H_2O_2) via SOD-catalyzed dismutation of $O_2^{\bullet-}$ (from I, step 1): $2 O_2^{\bullet-} + 2 H_2O → 2 OH^- + H_2O_2 + O_2 \uparrow$ (same as reaction 1) *Note*: The spontaneous dismutation of $O_2^{\bullet-}$ by H_2O has a rate constant ~2×10^5 M^{-1} s^{-1}, while that with SOD is 32,000-fold faster; 6.4×10^9 M^{-1} s^{-1} [52]. Step 3. Base (MeOH) formation: $Me^+ + OH^- → MeOH$

Table 2. *Cont.*

|	
II. Metal O_2^{2-} ($Me^+_2O_2^{2-}$, $Me^{2+}O_2^{2-}$, MeOOH); additional details for their hydrolysis are presented in reactions 4–6.	Step 1. Dissociation reaction of metal O_2^{2-} (e.g., $Me^+_2O_2^{2-}$): $Me^+_2O_2^{2-}$ (in H_2O) $\rightarrow O_2^{2-} + 2\,Me^+$ Step 2. Hydrolysis reaction of O_2^{2-} (from II, step 1): $O_2^{2-} + 2\,H_2O \rightarrow 2\,OH^- + H_2O_2$ (same as reaction 4) Step 3. Base (MeOH) formation: $2\,Me^{2+} + 2\,OH^- \rightarrow 2\,MeOH$
III. H_2O_2 released by the hydrolysis of metal $O_2^{\bullet-}$ and O_2^{2-}; additional details are shown in Figure 1 *step b*.	Release of O_2 via CAT-catalyzed decomposition of H_2O_2 [44], resulting from I, step 2, and/or II, step 2: $2\,H_2O_2 \rightarrow 2\,H_2O + O_2\uparrow$ (7)
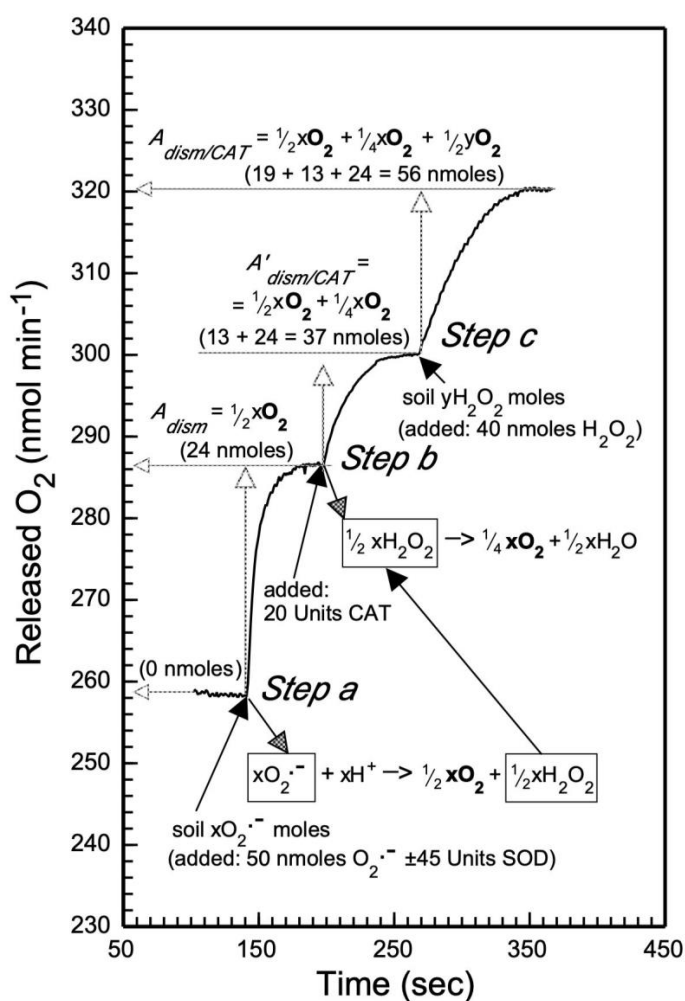
Figure 1. Simulation of the OxR (Oxygen Release) assay on $O_2^{\bullet-}$ and H_2O_2: It is performed in the presence/absence of Mars-like regolith from Mojave and Atacama deserts with a liquid-phase Clark-type O_2 electrode [49]. It is initiated (in *step a*) by the addition of 50 nmoles $O_2^{\bullet-}$ (simulating regolith $O_2^{\bullet-}$, represented as $x\,O_2^{\bullet-}$ moles) in the absence or presence of 45 units Cu/Zn-superoxide dismutase (SOD), and the concentration of released O_2 (by the SOD-catalyzed dismutation reaction of $O_2^{\bullet-}$) is recorded (as reading $A_{dism} = \frac{1}{2}xO_2$; see *Treatment A* in text), which is equal to the second dismutation reaction product H_2O_2 (= $\frac{1}{2}xH_2O_2$). In a subsequent *step b*, the addition of catalase (CAT) causes the additional release of O_2 (via the CAT-catalyzed decomposition of H_2O_2, the second product of $O_2^{\bullet-}$ dismutation), which is also recorded (as reading $A_{dism/CAT} = \frac{1}{4}xO_2$ plus the already released $\frac{1}{2}xO_2$; see *Treatment B* in text). If there are also metal O_2^{2-} or free H_2O_2 present in regolith (represented as yH_2O_2 moles), these are simulated in Figure 1 by the addition of 40 nmoles H_2O_2 (in *step c*). These peroxides will also be decomposed by the CAT (added in *step b*) to $\frac{1}{2}yO_2$, and in this case, the total released O_2 will be recorded in *step c* as reading $A_{dism/CAT}$ (the sum $\frac{1}{2}xO_2 + \frac{1}{4}xO_2 + \frac{1}{2}yO_2$).

4. OxR Assay Simulation Verification on Mars-Analog Regolith

The OxR assay was performed using a semi-sealed liquid-phase O_2 electrode with known concentrations of $O_2^{\bullet-}$ and H_2O_2, and in the presence/absence of Mars-like regolith from the Mojave (CIMA volcanic field) and the Atacama deserts. The assay was further validated on commercial sources of metal salts of $O_2^{\bullet-}$ (KO_2) and O_2^{2-} (Na_2O_2, CaO_2, MgO_2) in the presence of CO^{2-} and ClO_4^- (both are present in Martian regolith). *Gamma*-radiation experiments were performed to evaluate the stability of the OxR assay enzymes CAT and SOD against cosmic radiation [49].

The electrode reaction chamber was filled with 1 mL potassium (K)-phosphate-DTPA buffer (0.25 M K-phosphate buffer, pH 7.2, containing 10 mM DTPA) to which the assay reagents ($O_2^{\bullet-}$, H_2O_2, SOD, and CAT) were added at constant room temperature (RT). As already noted, DTPA chelates any soluble transition metal ions that can destroy H_2O_2 and $O_2^{\bullet-}$. Moreover, DTPA will also prevent such chelated metals from inactivating the OxR assay protein reagents SOD and CAT via their oxidation by $^{\bullet}OH$ (produced by way of the Fenton reaction) or via direct inhibition. The OxR assay was experimentally tested with known concentrations of $O_2^{\bullet-}$ and H_2O_2 added in the Clark-type O_2 electrode, as illustrated in Figure 1 [49]. To validate the OxR assay enzymatic reactions 1 and 7 (in Table 2) in the Clark-type O_2 electrode chamber, the following treatments were performed (data are shown in Figure 1):

Treatment A (reaction 1, see Figure 1 *step a*): SOD-catalyzed dismutation of $O_2^{\bullet-}$ to O_2 and H_2O_2). Seventy microliters of O_2^- stock solution was added (final 50 μM $O_2^{\bullet-}$ or 50 nmoles) to the O_2 electrode chamber, which contained 1 mL K-phosphate-DTPA buffer and ± 45 units (U) SOD (10 μl of a 4500 U ml^{-1} stock made in ddH$_2$O), and the released O_2 concentration was recorded until a plateau was reached.

Treatment B (reaction 7 in Table 2, see Figure 1 *step b*): CAT-catalyzed conversion to O_2 of H_2O_2 released via SOD-catalyzed dismutation $O_2^{\bullet-}$ derived by $O_2^{\bullet-}$ hydrolysis, and H_2O_2 released from peroxides via hydrolysis. After measuring the 1st O_2(g) plateau (*Treatment A*), 20 U ml^{-1} CAT (10 μl 2000 U ml^{-1} stock) was added to the resulting reaction mixture, and after the 2nd O_2(g) plateau was reached, 10 μl 4 mM H_2O_2 (final 40 μM or 40 nmoles) was added, and the 3rd O_2(g) plateau was recorded (Figure 1 *step c*).

Mathematical treatment of the data derived from treatments A and B: Assuming the presence of x $O_2^{\bullet-}$ and yH_2O_2 moles in the K-phosphate-DTPA buffer in the Clark O_2 electrode chamber, these supero/peroxidants were calculated from the experiments illustrated in Figure 1 as follows. The released O_2 concentrations measured by the O_2 electrode during *treatments A* and *B* (designated A_{dism} and $A_{dism/CAT}$, respectively) are described by the following molar equations and are based on the molar stoichiometry of the reactions 1 and 7 (in Table 2):

$A_{dism} = \frac{1}{2}xO_2$;

$$\text{simplified: } A_{dism} = \frac{1}{2}x, \text{ where } x \text{ is } O_2^{\bullet-} \text{ moles}$$

$A_{dism/CAT} = \frac{1}{2}xO_2 + \frac{1}{4}xO_2 + \frac{1}{2}yO_2$;

$$\text{simplified: } A_{dism/CAT} = \frac{3}{4}x + \frac{1}{2}y, \text{ where } y \text{ is } H_2O_2 \text{ moles}$$

The molar concentrations of $xO_2^{\bullet-}$ and yH_2O_2 are then estimated using the following mathematical equations, derived by appropriately combining the molar equations A_{dism} and $A_{dism/CAT}$:

$$O_2^{\bullet-} \text{ moles } (= x) = 2A_{dism}$$

$$H_2O_2 \text{ moles } (= y) = 2A_{dism/CAT} - 3A_{dism}$$

The released O_2 concentrations (A_{dism} and $A_{dism/CAT}$) during the OxR assay (shown in Figure 1) matched the concentrations predicted by the stoichiometry of each of the assay reactions 1 and 7. Indeed, when the values A_{dism} (corresponding to 24 nmoles from *step a*) and $A_{dism/CAT}$ (corresponding to

37 nmoles from *step b*, or 56 nmoles from *steps b* plus *c*) are inserted to the above molar equations for $O_2^{\bullet-}$ and H_2O_2, their calculated experimental concentrations are statistically equal to their concentrations which were added in the O_2 electrode chamber.

　　Simulation of cosmic radiation effect on the OxR assay enzymic reagents: Another consideration for the OxR instrument is whether its enzymatic reagents SOD and CAT would be functional upon exposure to cosmic radiation levels expected during missions to Mars, the Moon, and possibly icy satellites Jupiter and Saturn. To address this question for Mars and Moon, cosmic radiation simulation experiments were performed [49], where solid SOD and CAT were exposed to γ-radiation at a dose range comparable to that which would be received during a space mission. Activities were also determined for these enzymes in various concentrations (% v/v) of ACN since 100% ACN is used to wet the regolith sample to quantitatively purge out any unknown source trapped O_2. The SOD retained functional activity after exposure to a γ-radiation dose of 6 Gy (an equivalent to the cosmic radiation dose received from 38 round trips to Mars [53]). The CAT specific activity was unaffected up to ~3 Gy (equivalent to 19 round trips to Mars, and many more trips to the Moon) after which it decreased linearly to 40% (of its unexposed activity) at 6 Gy. SOD activity was unaffected in up to 50% ACN, while CAT activity decreased in a manner that matched the ACN concentration. For example, an initial CAT specific activity of ~3 U μg^{-1} at 0% ACN decreased by 50-fold at the maximum tested 50% ACN. This result indicates that for an OxR assay based on 3 U μg^{-1} CAT at 0% ACN in laboratory testing, the CAT concentration should be increased 50-fold (i.e., 150 U μg^{-1}) plus a margin for flight, if a 50% ACN concentration is optimum for instrument implementation.

5. The Potential of the OxR Assay for a Field-Deployable Instrument

　　The OxR assay can be extended to the search of possible metal supero/peroxidant cycles in terrestrial and extraterrestrial ecosystems. We expect that the full instrument can be packaged in 1 U (i.e., CubeSat sized at 10 cm/side) using a reaction chamber scheme with an O_2-sensor (to monitor the enzymatic release of O_2 from $O_2^{\bullet-}$ and O_2^{2-} in a regolith sample during interaction (under constant mixing) with SOD and CAT, as illustrated and described in Figure 2.

　　During operation, the first step of mixing the regolith with anhydrous ACN is very crucial for the following reasons: ACN (actually containing 0.2 mM dicyclohexano-18-crown-6 ether, CE) flushes loosely bound O_2 from unknown sources (designated zO_2) necessary for instrument calibration at the same time the CE component, will facilitate $O_2^{\bullet-}$ dissociation from superoxo metal salts [1,54,55], and together they stabilize $O_2^{\bullet-}$ for the subsequent enzymic steps 2 and 3 (Figure 2). In other words, the ACN-CE solvent used in step 1 prevents the dismutation of regolith $O_2^{\bullet-}$ to O_2 that would occur with the use of an aqueous solvent (see reaction 1 in Table 1), which would make the determination of background zO_2 (and, thus, of x $O_2^{\bullet-}$ and yH_2O_2 moles) impossible. It should also be noted that although the OxR assay can quantify O_2 released from unknown sources (i.e., zO_2), it cannot discriminate the H_2O_2 generated by the hydrolysis of metal superoxide radicals and peroxides from that of any free H_2O_2 (possibly existing in mineral pore spaces). The accurate quantification of metal superoxide radicals and peroxides by the OxR requires that their initial hydrolysis products $O_2^{\bullet-}$ and H_2O_2, respectively, remain stable for SOD and CAT treatment. It has been already noted, the metal chelator DTPA and the phosphate buffer reagents will scavenge inorganic cations that affect the stability of $O_2^{\bullet-}$ and H_2O_2. Even if a fraction of H_2O_2 converts to O_2 by factors other than CAT (e.g., by high CO^{2-} concentration and high regolith alkalinity [49], or by the catalysts MnO_2 [56], or silver, platinum, lead, ruthenate, and RuO_2, which decompose H_2O_2 to O_2 in alkaline solution [57]), this will not affect the accurate determination of metal superoxide radicals and peroxide concentrations since these factors will complement the conversion of H_2O_2 to O_2 by CAT.
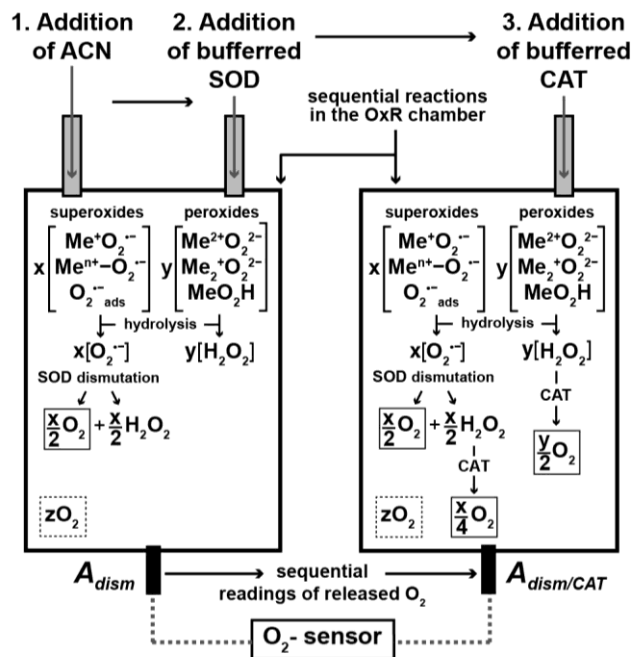
OxR instrument diagramatic principle

Figure 2. Diagrammatic principle of an OxR assay-based field instrument for the identification/quantification of regolith superoxide radicals and peroxides (shown as $xO_2^{\bullet-}$ and yH_2O_2 moles, respectively): Regolith sample is subjected to the following released O_2 recording procedures. In step 1, the regolith is wetted with anhydrous ACN to flush out loosely bound O_2 (designated zO_2 moles; enclosed in dotted squares) for (i) canceling out any background O_2 and (ii) measuring it as coming from unidentified sources. In step 2, SOD is administered in the instrument chamber dissolved in K-phosphate-DTPA buffer (pH = 7.2) at an equal (at least) to ACN volume (resulting in at least 50% ACN), and the released O_2 (enclosed in solid-line square, which results from the group of metal $O_2^{\bullet-}$ via SOD-catalyzed dismutation of their hydrolysis product $O_2^{\bullet-}$, together with H_2O_2) is recorded by the chamber O_2 sensor as reading A_{dism}. In a subsequent third step, K-phosphate-DTPA-buffered CAT is introduced in the same chamber, where the additional released O_2 (from the decomposition of H_2O_2 coming from the hydrolysis of both groups of metal $O_2^{\bullet-}$ and O_2^{2-}) is summed to that released from step 2 (and enclosed in three solid-line squares), and is recorded as reading $A_{dism/CAT}$. The values of A_{dism} and $A_{dism/CAT}$ (their net values determined by the experimental values designated by the arrows pointing at them on the Y-axis) are then used to determine the moles of regolith $O_2^{\bullet-}$ and H_2O_2, using their respective equations: $O_2^{\bullet-} = 2A_{dism}$ (= x), and $H_2O_2 = 2A_{dism/CAT}$ - $3A_{dism}$ (derived as shown in Section 4, 'OxR assay simulation verification on Mars-analog regolith').

Non-enzymatic OxR instrument version: We have also developed a non-enzymatic OxR assay for cases where enzymatic stability may be insufficient (e.g., missions to Titan, Europa, and Enceladus) or when the required long-term −20 °C SOD and CAT storage is not possible. Moreover, some future rovers may long outlast their expected life times (as past ones have done), and for whichever rover carries an OxR instrument the reagent enzymes may degrade over the years, whereas the inorganics may be more durable. A non-enzymatic version of the OxR instrument is based on the following reagents, which we have preliminarily tested successfully (data not shown):

In place of SOD, $CuSO_4$, $MnCl_2$, and $MnSO_4$ can be used:

1. $CuSO_4$ (at 0.1 to 300 μM) and $MnCl_2$ (at 0.1 to 100 μM)) [58,59]; $MnCl_2$ dismutates $O_2^{\bullet-}$ as effectively as SOD does [59].

2. $MnSO_4$ (at 0.1 mM) has a rate constant for $O_2^{\bullet-}$ dismutation $k = 2.3 \times 10^6$ M^{-1} s^{-1} (in 5 mM HEPES, pH = 7.8) [52]. This is 10-fold higher than the rate constant for the spontaneous aqueous dismutation of $O_2^{\bullet-}$ ($2\,O_2^{\bullet-} + 2\,H_2O \rightarrow 2\,OH^- + H_2O_2 + O_2$; $k = 2 \times 10^5$ M^{-1} s^{-1} at pH = 7.8 [60]).

In place of CAT, the following inorganic reagents can be used:

1. MnO_2 acts as CAT-mimetic ($2H_2O_2 \rightarrow 2H_2O + O_2$) [56].

2. Ferricyanide [$Fe(CN)_6^{3-}$; FECN]. FECN reacts with H_2O_2 at a different stoichiometry than that of its CAT-catalyzed decomposition [$\frac{1}{2}yH_2O_2 + Fe(CN)_6^{3-} \rightarrow Fe(CN)_6^{4-} + H^+ + \frac{1}{2}yO_2$ [61,62]]. However, the use of FECN modifies the set of the equations for the determination of $O_2^{\bullet-}$ and H_2O_2 via released O_2 (specifically the equation for H_2O_2). These are the following, designating as $A_{dism/FECN}$ as the reading value (by the O_2-electrode) for the released O_2 after treatment with FECN:

$$\mathbf{O_2^{\bullet-}} \text{ moles} = 2A_{dism} \text{ (same as with the enzymatic version of the OxR instrument)}$$

$$\mathbf{H_2O_2} \text{ moles} = A_{dism/FECN} - 2A_{dism}$$

Concluding, the principle of the OxR assay can be used for the development of an instrument for the detection of planetary and terrestrial $O_2^{\bullet-}$ and O_2^{2-} with the following considerations:

1. OxR assay enzymes SOD and CAT are used in excess; they are sufficient when used even in the amount of a few activity units.

2. SOD and CAT are stored (below −20 °C for long-term storage) separate from their aqueous solvents, and are mixed right before administration. This can be accomplished by storing them, for example, in two separate reagent crucibles (analogous to those used in the WCL instrument of the 2007 Phoenix Mars Scout Lander mission [63]), or in (commercially available) dual-chamber pre-fillable syringes (one chamber for storing the enzyme and one for its solvent, to be mixed upon piston movement), followed by their sequential dispensing in the instrument's regolith chamber (under continuous mixing of its reagents).

3. The instrument can use solid state electrochemical or optical sensing O_2-electrodes of high sensitivity. There are commercially available O_2 probes (e.g., sensor type PSt6, by PreSens Precision Sensing GmbH, Regensburg, Germany) that are based on the luminescence quenching by O_2, and are sensitive enough to measure O_2 at much lower concentrations (~1 nmole O_2 cm^{-3} regolith) than that (775 nmoles) detected by the GEX [26]. For example, the typical detection limit of the PreSens sensor PSt6 is 0.002% O_2, with 1 ppb and 0.5 ppm for aqueous and gaseous O_2, respectively. The PreSens Precision Sensing O_2 probes come either as needle-type optical fiber probes (with a tip size < 50 μm, protected, e.g., inside a stainless-steel needle), or as implantable probes (with a tip size of < 50 to 140 μm, while the outer diameter ranges from 140 μm to 900 μm). Therefore, O_2 sensing by the OxR instrument with solid-state sensors can be done in both gaseous and liquid phase. Regarding released O_2 partition between liquid and headspace in the sample chamber, underestimation of the released reactive O_2 due to such exsolution can be addressed by either adding an extra gas phase O_2 sensor, or by the calculation of the partition between liquid and gas phase at the set pressure and temperature.

4. Respective ACN and SOD reagent process steps 1 and 2 are omitted in testing water samples (e.g., from Enceladus and Europa) by the OxR instrument, because $O_2^{\bullet-}$ dismutates to H_2O_2 and O_2 under aqueous conditions (see reaction 1, Table 1). In such an application, the first step of the OxR instrument will record O_2 of unknown origin (for instrument calibration) in a melted ice sample. Following this step, CAT will be administered to convert to O_2 any present H_2O_2. This will be the only peroxidant specifically determined by the OxR instrument in the (melted) ice samples from the surface or plums of Enceladus and Europa.

6. Implementation of the OxR Instrument

One approach for implementing the OxR assay for field instrument construction is to keep it compatible with the Wet Chemistry Laboratory (WCL) that flew as part of the Phoenix lander mission to Mars [30]. The WCL (Figure 3) consists of a lower beaker containing sensors designed to analyze the

chemical properties of the regolith and an upper actuator assembly for adding regolith, water, reagents, and stirring [63]. The WCL sensor set included an O_2 electrode, pressure sensor, and thermocouple needed for the OxR assay. A key part of the WCL system is the storage of liquid and dry reagents. Our prototype design uses a reagent dispenser assembly similar to WCL (which uses five crucibles to store the reagents to be dispensed). We will use the following three crucibles:

A crucible for dispensing into the beaker the anhydrous ACN to wash out from regolith any background O_2 (for recording its level).

A crucible divided into two compartments to store the SOD enzyme and its solvent (for recording O_2 released from the dismutation of regolith superoxide radicals; H_2O_2 will also be released by this dismutation) separately.

A crucible divided into two compartments to store the CAT enzyme and its solvent (for recording O_2 released from superoxide radical-derived H_2O_2, and that derived from regolith peroxides) separately.
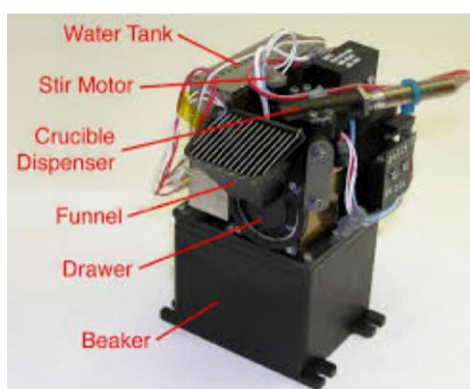

Figure 3. Image of the Wet Chemistry Laboratory (WCL) from the Phoenix Lander.

The automated and sequential dispensing of the reagents is critical to the success of the prototype. A diagram of the Phoenix system is shown in Figure 4. The reagent dispenser assembly will be coupled to the construction and operational testing of the beaker (reaction cell). A diagram of the WCL reaction cell is shown in Figure 5. In contrast to the complex array of sensors in the WCL on Phoenix [63], we have only O_2 sensors, temperature, and pressure. Joining the reagent dispenser assembly and the reaction cell completes the prototype. However, the WCL instrument uses a 25-cc chamber to analyze 1 cc of regolith. For some missions, this is an important issue and motivates microfluidics approaches. An alternative instrument construction approach will be based on the microfluidic transport/delivery technology [64–69], already developed by the R.A. Mathies's Space Sciences Laboratory at Berkeley University. The chip for microscopic fluid transport between the components of an instrument such as OxR (e.g., reagent storage capsules, regolith sample chamber with O_2/temp/pressure sensors, and waste reservoirs), is analogous to digital electronic processors, and all that is needed is a change in the order of operations conducted by the device [66]. All macroscopic reagent volumes are contained within stainless steel bellows expanded or contracted by externally applied N_2 gas. The OxR instrument chip can be constructed as a scaled-down version (e.g., a 200 gr, 2 Watts, 10x10x10 cm package) of the Enceladus Organic Analyzer (EOA) chip (Figure 6).

The OxR instrument prototype will be tested in a laboratory setting and results compared to standard laboratory procedures, followed by field testing in the Mojave Desert. This has been a continuing test site for our studies [1], and, thus, we have a deep knowledge base of the site and the expected results providing a convenient basis for prototype testing.
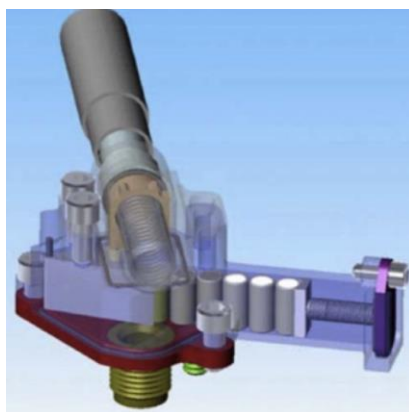
Figure 4. Diagram of the reagent dispenser assembly with crucibles ready for deployment [63].
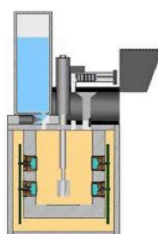
Figure 5

Figure 5. Diagram of the WCL reaction cell showing water storage and stirring rod.
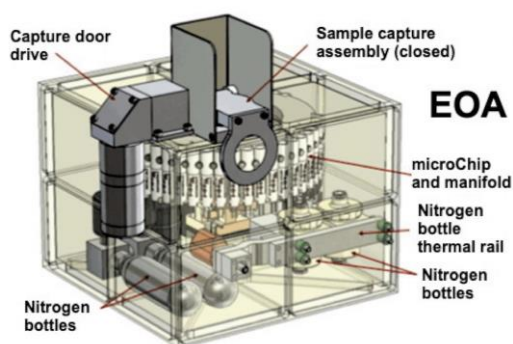
Figure 6

Figure 6. Diagram of the Enceladus Organic Analyzer (EOA) data programmable chip (modified from [65]).

7. Studies with the OxR Instrument

The OxR instrument can have the following potential applications:

Identification of the ROS $O_2^{\bullet-}$ and O_2^{2-}, on the Moon and Mars, with extension to future missions to Jupiter's satellite Europa and Saturn's Enceladus and Titan.

Monitor the levels of ROS for astronaut health and safety, given that $O_2^{\bullet-}$ can become biotoxic (via conversion of Fe^{3+}/Cu^{2+} to Fe^{2+}/Cu^+, which, via the Fenton-reaction with the other ROS $O_2^{\bullet-}$, will generate the highly biotoxic free radical $^\bullet OH$ [44]). Moreover, measuring dust/silica-induced ROS generation is crucial for the evaluation of possible health hazards [18] in future manned missions to Mars and Moon.

Identify mineral deposits rich in ROS to be used as an O_{2g} source for human consumption. O_{2g} can be easily produced on a large scale due to the following ROS reactions: $O_2^{\bullet-}$ is converted to O_{2g} by mixing with (i) H_2O (also releasing H_2O_2), or (ii) Fe^{3+} or Cu^{2+} [44]. O_{2g} can be produced from

O_2^{2-} (e.g., H_2O_2 also released from reaction (i)) by mixing with MnO_2 [56] or silver, platinum, lead, ruthenate, or RuO_2 [57].

Identify $O_2^{\bullet-}/O_2^{2-}$ on the metal parts of manned space vehicles/stations. ROS can be generated by a combination of O_{2g} (in vehicle) with cosmic radiation [1]. $O_2^{\bullet-}$ and O_2^{2-} have implications for exploration because they can:

(i) cause corrosive oxidative deterioration of space vehicles/stations,

(ii) pose a serious risk for oxidative modification of stored foods, making them unsafe for astronauts,

(iii) compromise astronaut health due to their well-known biotoxic effects [44].

Identify locations on Mars and the Moon with low ROS levels which may be indicative of the high potential for biosignature (e.g., [70,71]) preservation. Of particular upcoming interest is the Dragonfly mission to Titan by NASA (launched in 2026, and landing in 2034), which will search for evidence of prebiotic chemical processes on the surface of Titan [72].

The instrument is also applicable to terrestrial research, with indicative studies being: (i) $O_2^{\bullet-}/O_2^-$ association to microorganisms' oxidative stress in extreme desert environments, with extension to life's origin [1,73]; (ii) health hazard implications from measuring ROS-reactivity of (a) volcanic ash (due to $^\bullet OH$ generation) [74], and (b) pyrites (from $O_2/H_2O_2/$surface-bound ferric iron-induced $^\bullet OH$ generation during pyrite oxidation) in coal mining regions [75].

8. Conclusions

We have developed a sensitive assay for the use in a future Oxygen Release (OxR) instrument for the detection of ROS, with potential applications to the Mars, Moon, Europa, Titan, and Enceladus missions. The instrument can support the exploration of the Moon (including monitoring of astronaut health hazards), exploration on Mars, Moon, and Titan, and terrestrial studies. The OxR instrument is based on the selective and specific enzymatic decomposition of supero/peroxidants to O_2 and their quantification by the measurement of the released O_2. An alternative non-enzymatic option is also proposed. Laboratory simulations and the sensitivity of the commercially available O_2 sensors indicate that the OxR instrument can detect metal $O_2^{\bullet-}/O_2^{2-}$ in the Martian and Lunar regolith and also O_2^{2-} in the icy waters of the satellites of Saturn Enceladus and Titan (in its regolith too) and of Jupiter's Europa, at levels as low as 10 ppb. In terms of Technology Readiness Level, the OxR instrument is at 3 (method validated in the lab), and can be made flight-ready by leveraging the Phoenix Wet Chemical Laboratory hardware or a microfluidic transport/delivery technology.

References

1. Georgiou, C.D.; Sun, H.J.; McKay, C.P.; Grintzalis, K.; Papapostolou, I.; Zisimopoulos, D.; Panagiotidis, K.; Zhang, G.; Koutsopoulou, E.; Christidis, G.E.; et al. Evidence for photochemical production of reactive oxygen species in desert soils. *Nat. Commun.* **2015**, *6*, 7100. [CrossRef] [PubMed]

2. Barker, E.S. Detection of molecular oxygen in the Martian atmosphere. *Nature* **1972**, *238*, 447–448. [CrossRef]

3. Feldman, P.D.; Morrison, D. The Apollo 17 Ultraviolet Spectrometer: Lunar atmosphere measurements revisited. *Geophys. Res. Lett.* **1991**, *18*, 2105–2109. [CrossRef]

4. Stern, A.S. The Lunar atmosphere: History, status, current problems, and context. *Rev. Geophys.* **1999**, *37*, 453–491. [CrossRef]

5.   Hall, D.T.; Strobel, D.F.; Feldman, P.D.; Mcgrath, M.A.; Weaver, H.A. Detection of an oxygen atmosphere on Jupiter's moon Europa. *Nature* **1995**, *373*, 677–679. [CrossRef] [PubMed]

6.   Johnson, R.E.; Luhmann, J.G.; Tokar, R.L.; Bouhram, M.; Berthelier, J.J.; Sittler, E.C.; Cooper, J.F.; Hill, T.W.; Smith, H.T.; Michael, M.; et al. Production, ionization and redistribution of O_2 in Saturn's ring atmosphere. *Icarus* **2006**, *180*, 393–402. [CrossRef]

7.   Goldsmith, P.F.; Liseau, R.; Bell, T.A.; Black, J.H.; Chen, J.-H.; Hollenbach, D.; Kaufman, M.J.; Li, D.; Lis, D.C.; Melnick, G.; et al. Herschel measurements of molecular oxygen in Orion. *Astrophys. J.* **2011**, *737*, 96. [CrossRef]

8.   Yao, Y.; Shushkov, P.; Miller, T.F., III; Giapis, K.P. Direct dioxygen evolution in collisions of carbon dioxide with surfaces. *Nat. Commun.* **2019**, *10*, 2294. [CrossRef]

9.   Schwadron, N.A.; Baker, T.; Blake, B.; Case, A.W.; Cooper, J.F.; Golightly, M.; Jordan, A.; Joyce, C.; Kasper, J.; Kozarev, K.; et al. Lunar radiation environment and space weathering from the Cosmic Ray Telescope for the effects of radiation (CRaTER). *J. Geophys. Res.* **2012**, *117*, E00H13. [CrossRef]

10.   Turci, F.; Corazzari, I.; Alberto, G.; Martra, G.; Fubini, B. Free-radical chemistry as a means to evaluate Lunar dust health hazard in view of future missions to the moon. *Astrobiology* **2015**, *15*, 371–380. [CrossRef]

11.   Hendrix, D.A.; Port, S.T.; Hurowitz, J.A.; Schoonen, M.A. Measurement of OH * generation by pulverized minerals using Electron Spin Resonance spectroscopy and implications for the reactivity of planetary regolith. *GeoHealth* **2019**, *3*, 28–42. [CrossRef]

12.   Hurowitz, J.A.; Tosca, N.J.; McLennan, S.M.; Schoonen, M.A.A. Production of hydrogen peroxide in Martian and Lunar soils. *Earth Planet. Sci. Lett.* **2007**, *255*, 41–52. [CrossRef]

13.   Linnarsson, D.; Carpenter, J.; Fubini, B.; Gerde, P.; Karlsson, L.L.; Loftus, D.J.; Prisk, G.K.; Staufer, U.; Tranfield, E.M.; van Westrenen, W. Toxicity of Lunar dust. *Planet. Space Sci.* **2012**, *74*, 57–71. [CrossRef]

14.   Wallace, W.T.; Phillips, C.J.; Jeevarajan, A.S.; Chen, B.; Taylor, L.A. Nanophase iron-enhanced chemical reactivity of ground Lunar soil. *Earth Planet. Sci. Lett.* **2010**, *295*, 571–577. [CrossRef]

15.   Bak, E.N.; Zafirov, K.; Merrison, J.P.; Jensen, S.J.K.; Nørnberg, P.; Gunnlaugsson, H.P.; Finster, K. Production of reactive oxygen species from abraded silicates. Implications for the reactivity of the Martian soil. *Earth Planet Sci. Lett.* **2017**, *473*, 113–121. [CrossRef]

16.   Hasegawa, M.; Ogata, T.; Sato, M. Mechano-radicals produced from ground quartz and quartz glass. *Powder Technol.* **1995**, *85*, 269–274. [CrossRef]

17.   Fubini, B.; Hubbard, A. Reactive Oxygen Species (ROS) and Reactive Nitrogen Species (RNS) generation by silica in inflammation and fibrosis. *Free Rad. Biol. Med.* **2003**, *34*, 1507–1516. [CrossRef]

18.   Caston, R.; Luc, K.; Hendrix, D.; Hurowitz, J.A.; Demple, B. Assessing toxicity and nuclear and mitochondrial DNA damage caused by exposure of mammalian cells to Lunar regolith simulants. *GeoHealth* **2018**, *2*, 139–148. [CrossRef]

19.   Cooper, J.F.; Cooper, P.D.; Sittler, E.C.; Sturner, S.J.; Rymer, A.M. Old faithful model for radiolytic gas-driven cryovolcanism at Enceladus. *Planet. Space Sci.* **2009**, *57*, 1607–1620. [CrossRef]

20.   Sittler, E.C.; Ali, A.; Cooper, J.F.; Hartle, R.E.; Johnson, R.E.; Coates, A.J.; Young, D.T. Heavy ion formation in Titan's ionosphere: Magnetospheric introduction of free oxygen and a source of Titan's aerosols? *Planet. Space Sci.* **2009**, *57*, 1547–1557. [CrossRef]

21.   Gaidos, E.J.; Nealson, K.H.; Kirschvink, J.L. Life in Ice-Covered Oceans. *Science* **1999**, *284*, 1631–1633. [CrossRef] [PubMed]

22.   Hand, K.P.; Carlson, R.W.; Chyba, C.F. Energy, chemical disequilibrium, and geological constraints on Europa. *Astrobiology* **2007**, *7*, 1006–1022. [CrossRef] [PubMed]

23.   Klein, H.P. The Viking biological experiments on Mars. *Icarus* **1978**, *34*, 666–674. [CrossRef]

24.   Zent, A.P.; McKay, C.P. The chemical reactivity of the Martian soil and implications for future missions. *Icarus* **1994**, *108*, 146–457. [CrossRef]

25.   Quinn, R.C.; Martucci, H.F.; Miller, S.R.; Bryson, C.E.; Grunthaner, F.J.; Grunthaner, P.J. Perchlorate radiolysis on Mars and the origin of Martian soil reactivity. *Astrobiology* **2013**, *13*, 515–520. [CrossRef] [PubMed]

26.   Oyama, V.I.; Berdahl, B.J.; Carle, G.C. Preliminary findings of the Viking Gas Exchange Experiment and a model for Martian surface chemistry. *Nature* **1977**, *265*, 110–114. [CrossRef]

27.   Klein, H.P.; Horowitz, N.H.; Levin, G.V.; Oyama, V.I.; Lederberg, J.; Rich, A.; Hubbard, J.S.; Hobby, G.L.; Straat, P.A.; Berdahl, B.J.; et al. The Viking biological investigation: Preliminary results. *Science* **1976**, *194*, 99–105. [CrossRef] [PubMed]

28. Levin, G.V.; Straat, P.A. Viking Labeled Release biology experiment: Interim results. *Science* **1976**, *194*, 1322–1329. [CrossRef]

29. Yen, A.S.; Kim, S.S.; Hecht, M.H.; Frant, M.S.; Murray, B. Evidence that the reactivity of the Martian soil is due to superoxide ions. *Science* **2000**, *289*, 1909–1912. [CrossRef]

30. Hecht, M.H.; Kounaves, S.P.; Quinn, R.C.; West, S.J.; Young, S.M.M.; Ming, D.W.; Catling, D.C.; Clark, B.C.; Boynton, W.V.; Hoffman, J.; et al. Detection of perchlorate and the soluble chemistry of Martian soil at the Phoenix Lander site. *Science* **2009**, *325*, 64–67. [CrossRef]

31. Navarro-González, R.; Vargas, E.; de la Rosa, J.; Raga, A.C.; McKay, C.P. Reanalysis of the Viking results suggests perchlorate and organics at mid-latitudes on Mars. *J. Geophys. Res.* **2010**, *115*, E12010.

32. Glavin, D.P.; Freissinet, C.; Miller, K.E.; Eigenbrode, J.L.; Brunner, A.E.; Buch, A.; Sutter, B.; Archer, P.D.J.; Atreya, S.K.; Brinckerhoff, W.B.; et al. Evidence for perchlorates and the origin of chlorinated hydrocarbons detected by SAM at the Rocknest aeolian deposit in Gale Crater. *J. Geophs. Res.* **2013**, *118*, 1–19.

33. Prince, L.A.; Johnson, E.R. The radiation-induced decomposition of the alkali and alkaline earth perchlorates. I. Product yields and stoichiometry. *J. Phys. Chem.* **1965**, *69*, 359–377. [CrossRef]

34. Georgiou, C.D.; Zisimopoulos, D.; Kalaitzopoulou, E.; Quinn, R.C. Radiation driven formation of reactive oxygen species in oxychlorine containing Mars surface analogues. *Astrobiology* **2017**, *17*, 319–336. [CrossRef]

35. Lasne, J.; Noblet, A.; Szopa, C.; Navarro-González, R.; Cabane, M.; Poch, O.; Stalport, F.; François, P.; Atreya, S.K.; Coll, P. Oxidants at the surface of Mars: A review in light of recent exploration results. *Astrobiology* **2016**, *16*, 977–996. [CrossRef]

36. McKay, C.P.; Grunthaner, F.J.; Lane, A.L.; Herring, M.; Bartman, R.K.; Ksendzov, A.; Manning, C.M.; Lamb, J.L.; Williams, R.M.; Ricco, A.J.; et al. The Mars Oxidant Experiment (MOX) for Mars' 96. *Planet. Space Sci.* **1998**, *46*, 769–777. [CrossRef]

37. Sharma, R.K. Peroxides, peracides and their salts. In *Inorganic Reaction Mechanisms*; Discovery Publishing House: New Delhi, India, 2007; pp. 132–173.

38. Lunsford, J.H. ERS of adsorbed oxygen species. *Catal. Rev.* **1973**, *8*, 135–157. [CrossRef]

39. Dyrek, K.; Che, M. EPR as a tool to investigate the transition metal chemistry on oxide surfaces. *Chem. Rev.* **1997**, *97*, 305–331. [CrossRef]

40. Makarov, S.Z.; Ladelnova, L.V. The peroxides of titanium, zirconium, and cerium formed in the reaction of their hydroxides with hydrogen peroxide. *Rus. Chem. Bull.* **1961**, *10*, 889–893. [CrossRef]

41. Kounaves, S.P.; Hecht, M.H.; Kapit, J.; Gospodinova, K.; DeFlores, L.; Quinn, R.C.; Boynton, W.V.; Clark, B.C.; Catling, D.C.; Hredzak, P.; et al. Wet chemistry experiments on the 2007 Phoenix Mars Scout Lander mission: Data analysis and results. *J. Geophys. Res.* **2010**, *115*, E00E10. [CrossRef]

42. Quinn, R.C.; Chittenden, J.D.; Kounaves, S.P.; Hecht, M.H. The oxidation-reduction potential of aqueous soil solutions at the Mars Phoenix landing site. *Geophys. Res. Lett.* **2011**, *38*, L14202. [CrossRef]

43. Dukes, C.A.; Baragiola, R.A. The Lunar surface-exosphere connection: Measurement of secondary-ions from Apollo soils. *Icarus* **2015**, *255*, 51–57. [CrossRef]

44. Halliwell, B.; Gutteridge, J.M.C. *Free Radicals in Biology and Medicine*, 5th ed.; Oxford University Press: Oxford, UK, 2015; p. 904.

45. NASA. Forward to the Moon: NASA's STRATEGIC Plan for Lunar Exploration. 23 May 2019. Available online: https://www.nasa.gov/sites/default/files/atoms/files/america_to_the_moon_2024_artemis_20190523.pdf (accessed on 20 August 2019).

46. Allen, C.C.; Morris, R.V.; LJager, K.M.; Golden, D.C.; Lindstrom, D.J.; Lindstrom, M.M.; Lockwood, J.P. Martian Regolith Simulant JSC Mars-1. In Proceedings of the Lunar and Planetary Science XXIX: Papers Presented to the Twenty-Ninth Lunar and Planetary Science Conference, Houston, TX, USA, 16–20 March 1998.

47. Peters, G.H.; Abbey, W.; Bearman, G.H.; Mungas, G.S.; Smith, J.A.; Anderson, R.C.; Douglas, S.; Beegle, L.W. Mojave Mars simulant—Characterization of a new geologic Mars analog. *Icarus* **2008**, *197*, 470–479. [CrossRef]

48. Slyuta, E.N. Physical and mechanical properties of the Lunar soil. *Solar System Res.* **2014**, *48*, 330–353. [CrossRef]

49. Georgiou, C.D.; Zisimopoulos, D.; Panagiotidis, K.; Grintzalis, K.; Papapostolou, I.; Quinn, R.C.; McKay, C.P.; Sun, H. Martian superoxide and peroxide O_2 Release (OR) assay: A new technology for terrestrial and planetary applications. *Astrobiology* **2016**, *16*, 126–142. [CrossRef]

50. Kelly, K.J.; Sandoval, R.M.; Dunn, K.W.; Molitoris, B.A.; Dagher, P.C. A novel method to determine specificity and sensitivity of the Tunel reaction in the quantitation of apoptosis. *Am. J. Physiol. Cell Physiol.* **2003**, *284*, C1309–C1318. [CrossRef]

51. Haber, F.; Weiss, J. Über die katalyse des hydroperoxydes. *Naturwissenschaften* **1932**, *20*, 948–950. [CrossRef]

52. Gray, B.; Carmichael, A.J. Kinetics of superoxide scavenging by dismutase enzymes and manganese mimics determined by Electron Spin Resonance. *Biochem. J.* **1992**, *281*, 795–802. [CrossRef]

53. Zeitlin, C.; Hassler, D.M.; Cucinotta, F.A.; Ehresmann, B.; Wimmer-Schweingruber, R.F.; Brinza, D.E.; Kang, S.; Weigle, G.; Böttcher, S.; Böhm, E.; et al. Measurements of energetic particle radiation in transit to Mars on the Mars Science Laboratory. *Science* **2013**, *340*, 1080–1084. [CrossRef]

54. Mishra, B.; Priyadarsini, K.I.; Bhide, M.K.; Kadam, R.M.; Mohan, H. Reactions of superoxide radicals with curcumin: Probable mechanisms by Optical Spectroscopy and EPR. *Free Radic. Res.* **2004**, *38*, 355–362. [CrossRef]

55. Afanasev, B.; Kuprianova, N.; Polozova, N. Kinetics and mechanism of the reactions of the superoxide ion in solutions. I. Absorption spectra and interaction with solvents and cations. *Int. J. Chem. Kinet.* **1983**, *15*, 1045–1056. [CrossRef]

56. Do, S.-H.; Batchelor, B.; Lee, H.-K.; Kong, S.-H. Hydrogen peroxide decomposition on manganese oxide (pyrolusite): Kinetics, intermediates, and mechanism. *Chemosphere* **2009**, *75*, 8–12. [CrossRef]

57. Venkatachalapathy, R.; Davila, G.P.; Prakash, J. Catalytic decomposition of hydrogen peroxide in alkaline solutions. *Electrochem. Commun.* **1999**, *1*, 614–617. [CrossRef]

58. MacKenzie, A.; Martin, W. Loss of endothelium-derived nitric oxide in rabbit aorta by oxidant stress: Restoration by superoxide dismutase mimetics. *Br. J. Pharmacol.* **1998**, *124*, 719–728. [CrossRef]

59. Mok, L.S.J.; Paisley, K.; Martin, W. Inhibition of nitrergic neurotransmission in the bovine retractor penis muscle by an oxidant stress: Effects of superoxide dismutase mimetics. *Br. J. Pharmacol.* **1998**, *124*, 111–118. [CrossRef]

60. Behar, D.; Czapski, G.; Rabani, J.; Dorfman, L.M.; Schwarz, H.A. The acid dissociation constant and decay kinetics of the perhydroxyl radical. *J. Phys. Chem.* **1970**, *74*, 3209–3213. [CrossRef]

61. Hughes, G.; Willis, C. Scavenger studies in the radiolysis of aqueous ferricyanide solutions at high pH. *Discuss. Faraday Soc.* **1963**, *36*, 223–231. [CrossRef]

62. Woodbury, W.; Spencer, A.K.; Stahmann, M.A. An improved procedure using ferricyanide for detecting catalase isozymes. *Anal. Biochem.* **1971**, *44*, 301–305. [CrossRef]

63. Kounaves, S.P.; Hecht, M.H.; West, S.J.; Morookian, J.-M.; Young, S.M.M.; Quinn, R.C.; Grunthaner, P.; Wen, X.; Weilert, M.; Cable, C.A.; et al. The MECA Wet Chemistry Laboratory on the 2007 Phoenix Mars Scout Lander. *J. Geophys. Res.* **2009**, *114*, E00A19. [CrossRef]

64. Duca, Z.A.; Tan, G.K.; Cantrell, T.; van Enige, M.; Dorn, M.; Cato, M.; Speller, N.C.; Pital, A.; Mathies, R.A.; Stockton, A.M. Operation of pneumatically-actuated membrane-based microdevices for in situ analysis of extraterrestrial organic molecules after prolonged storage and in multiple orientations with respect to Earth's gravitational field. *Sens. Actuators B Chem.* **2018**, *272*, 229–235. [CrossRef]

65. Mathies, R.A.; Razu, M.E.; Kim, J.; Stockton, A.B.; Turin, P.; Butterworth, A. Feasibility of detecting bioorganic compounds in Enceladus plumes with the Enceladus Organic Analyzer (EOA). *Astrobiology* **2017**, *17*, 902–912. [CrossRef] [PubMed]

66. Kim, J.; Stockton, A.M.; Jensen, E.C.; Mathies, R.A. Pneumatically actuated microvalve circuits for programmable automation of chemical and biochemical analysis. *Lab Chip* **2016**, *16*, 812–819. [CrossRef] [PubMed]

67. Linshiz, G.; Jensen, E.; Stawski, N.; Bi, C.; Elsbree, N.; Jiao, H.; Kim, J.; Mathies, R.; Keasling, J.D.; Hillson, N.J. End-to-end automated microfluidic platform for synthetic biology: From design to functional analysis. *J. Biol. Eng.* **2016**, *10*, 3. [CrossRef] [PubMed]

68. Geng, T.; Mathies, R.A. Forensic typing of single cells using droplet microfluidics. In *Microfluidic Methods for Molecular Biology*; Lu, C., Verbridge, S.S., Eds.; Springer International Publishing: Cham, Switzerland, 2016; pp. 71–94.

69. Jung, Y.K.; Kim, J.; Mathies, R.A. Microfluidic linear hydrogel array for multiplexed single nucleotide polymorphism (snp) detection. *Anal. Chem.* **2015**, *87*, 3165–3170. [CrossRef] [PubMed]

70. Georgiou, C.D.; Deamer, D.W. Lipids as universal biomarkers of extraterrestrial life. *Astrobiology* **2014**, *14*, 541–549. [CrossRef]

71. Georgiou, C.D. Functional properties of amino acid side chains as biomarkers of extraterrestrial life. *Astrobiology* **2018**, *18*, 1479–1496. [CrossRef] [PubMed]

72. NASA. NASA's Dragonfly Will Fly around Titan Looking for Origins, Signs of Life. 27 June 2019. Available online: https://www.nasa.gov/press-release/nasas-dragonfly-will-fly-around-titan-looking-for-origins-signs-of-life (accessed on 20 August 2019).

73. Deamer, W.D.; Georgiou, C.D. Hydrothermal conditions and the origin of cellular life. *Astrobiology* **2015**, *15*, 1091–1095. [CrossRef]

74. Horwell, C.J.; Fenoglio, I.; Vala Ragnarsdottir, K.; Sparks, R.S.; Fubini, B. Surface reactivity of volcanic ash from the eruption of Soufriere Hills volcano, Montserrat, West Indies with implications for health hazards. *Environ. Res.* **2003**, *93*, 202–215. [CrossRef]

75. Schoonen, M.A.A.; Harrington, A.D.; Laffers, R.; Strongin, D.R. Role of hydrogen peroxide and hydroxyl radical in pyrite oxidation by molecular oxygen. *Geochim. Cosmochim. Acta* **2010**, *74*, 4971–4987. [CrossRef]